NOAA ROSES Semi-Annual Report

Reporting Period: September 2021 – February 2022 (3rd report)

PI: Prof. Ping Yang (Texas A&M University)

Co-PI(s): Prof. Xianglei Huang (University of Michigan)

Project Title: Utilizing geostationary satellite observations to develop a next-generation ice cloud optical property model in support of JCSDA Community Radiative Transfer Model (CRTM) and JPSS CAL/VAL

Executive Summary (1 paragraph max)

This semi-annual report contains two parts: The first part summarizes the research progress of the Texas A&M University team led by Prof. Ping Yang, and the second part summarizes the research progress of the University of Michigan Co-I, Prof. Xianglei Huang.

Progress toward FY21 Milestones and Relevant Findings (with any Figs)

Texas A&M University team's accomplishments:

Task A—Development of the next-generation ice optical property model

- The single-scattering property computations for a preliminary version of the next-generation ice optical property model.
- The development of ice particle habit distributions for a preliminary version of the next-generation ice optical property model.

Task B—Development of computer programs for the consistency evaluations of the next-generation ice optical property model

- Spectral consistency procedure.
- Active-passive consistency procedure.

The University of Michigan team's accomplishments:

The University of Michigan (UM) team has kept working on evaluation of the CRTM 2.4.0 so its performance on Advanced Baseline Imager (ABI) radiance simulation can be better understood.

1. The single-scattering property computations for a preliminary version of the next-generation ice optical property model

We computed the single-scattering properties of 83 ice crystal shape models at wavelengths ranging from ultraviolet (UV) to microwave (0.2–200,000 μm) with particle diameters 2–10,000 μm. The 83 ice crystal shape models include 63 single hexagonal columns with nine aspect ratios (0.1–10) and seven surface roughnesses (0.0–0.5), and 20 irregular column aggregates, illustrated in Fig. 1. We split the spectral domains into six spectral regimes (wavelength boundaries listed in Table 1; abbreviations are ultraviolet-visible [UV-VIS], near-infrared [NIR], shortwave IR [SWIR], thermal IR [TIR], sub-millimeter [SUBM], and microwave [MCRW]). To minimize the computational requirement, we computed the single-scattering properties of ice crystals for various size parameters with each pair of the complex refractive index parameters in each wavelength domain, instead of one set of all diameter and wavelength combinations. The scattering property computations are stored with the kernel technique (Saito et al., 2021) to minimize the data volume.
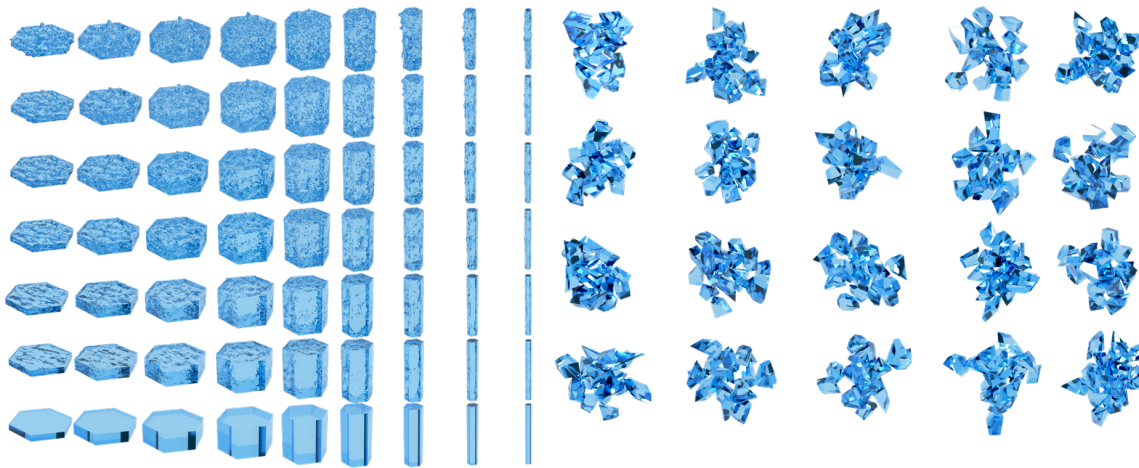
Figure 1. Ice crystal shape models to be used for the next-generation ice optical property model. The 63 single hexagonal columns include various particle aspect ratios 0.1–10 and degrees of surface roughness 0–0.5. The 20 irregular column aggregate models are consistent with Loeb et al. (2018).

Table 1 lists the single-scattering database's configurations (wavelength, size parameter, and refractive index). The scattering property computations are performed with the Invariant-Imbedding T-matrix Method (IITM; Bi et al., 2013), Improved Geometric Optics Method (IGOM; Yang and Liou, 1996), and Physical Geometric Optics Method (PGOM; Yang and Liou, 1997; Bi et al., 2011). We have completed IITM computations for size parameters less than 75–100 (depending on the spectral regime) and IGOM for larger particles. Nearly 40% of the PGOM computations for the backscattering directions of aggregate particles in the UV-VIS regime have

been completed as of January 31, 2022. Note that the PGOM computations for aggregate particles require substantial computational time but are essential for active-passive consistency in ice cloud optical thickness retrievals.

Table 1. General configuration of the database (λ = wavelength, x = size parameter, m_r = real part of refractive index, m_i = imaginary part of refractive index, N_x = number of size parameter values in database within this wavelength band, and N_m_r, N_m_i = number of corresponding m_r and m_i values within this wavelength band).

	UV-VIS	NIR	SWIR	TIR	SUBM	MCRW
λ_{min}	0.17 µm	0.95 µm	1.45 µm	2.7 µm	85 µm	1000 µm
λ_{max}	0.95 µm	1.45 µm	2.7 µm	85 µm	1000 µm	200000 µm
x_{min}	10	6.81292	3.16228	0.1	<0.01	<0.01
x_{max}	383119	100000	68129.2	31622.8	1000	100
N_x	74	71	77	91	85	67
m_{r_min}	1.298538	1.281838	1.141254	0.9	1.749894	1.749894
m_{r_max}	1.398107	1.316228	1.316228	2.0	1.891251	1.794328
N_m_r	6	3	8	29	4	2
m_{i_min}	1.0e-11	3.16228e-7	1.0e-4	1.0e-3	1.33352e-3	1.0e-6
m_{i_max}	1.0e-6	3.16228e-4	3.16228e-3	1.77828	3.16228e-1	1.0e-2
N_m_i	4	13	13	14	20	33

2. The development of ice particle habit distributions for a preliminary version of the next-generation ice optical property model

In this bulk ice optical property model development, we use observational and theoretical constraints on ice particle habit distributions (PHD). A number of in-situ observational studies have revealed that ice crystal shape characteristics have a dependence on the ambient atmospheric environment, such as air temperature (Heymsfield et al., 2002). Also, the vapor growth rate on each aspect of the ice crystal surface has temperature dependence (Harrington et al., 2021). Recent direct measurements of the surface of ice crystals with a scanning electron microscope quantify the degree of surface roughness of ice crystals through cloud chamber experiments (Neshyba et al., 2013; Butterfield et al., 2017). Also, the fraction of aggregate particles among ice crystals can be empirically obtained using in-situ measured particle mass diameter and ice water content (Baum et al., 2005; Loeb et al., 2018). We have developed a

preliminary bulk PHD model, as part of the next-generation ice optical property model development, by exploiting such resources and knowledge as depicted in Fig. 2. In the preliminary version, we incorporate the following characteristics:

- Log-normal distribution of the particle surface roughness with median surface roughness of 0.15, invariant to temperature and particle size;
- A size-dependent aggregate particle fraction modified from that of Loeb et al. (2018);
- A temperature-dependent aspect ratio distributions constraint with Harrington et al. (2021) (Fig. 2, a center of the right panels).

For the particle size distributions (PSD), we use the gamma distribution with an effective variance of 0.1. After the PSD and PHD are determined, we compute the bulk optical properties from the single-scattering properties of ice crystals available from the showcase (Fig. 2).
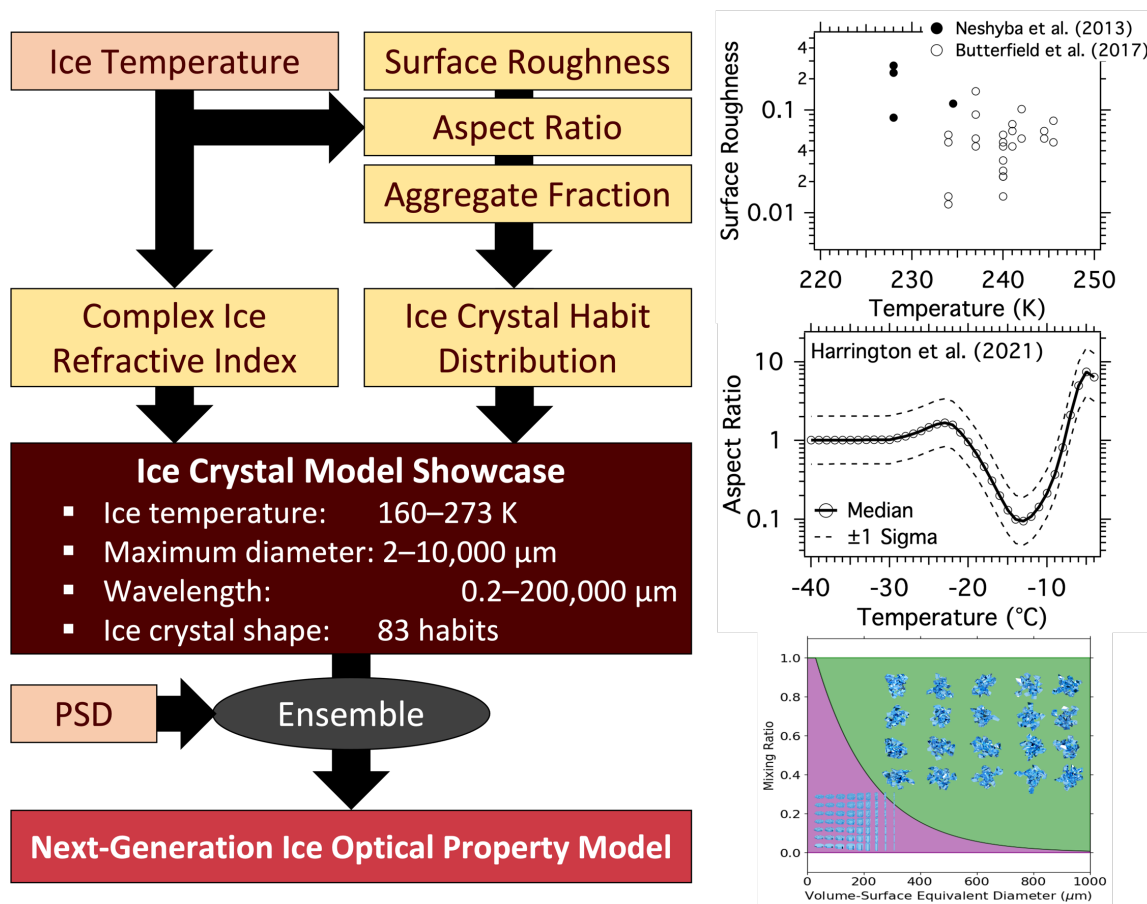
Figure 2. A flow chart of the bulk particle habit distribution and optical property computational procedure. The ice body temperature determines the spectral complex refractive index of ice crystals and aspect ratio distributions of single hexagonal crystals. In addition, the size-dependent aggregate fractions and size-invariant surface roughness distributions are predetermined. We mix the 83 ice crystal shape models from these ice crystal shape characteristics to make a weighted ensemble mean of ice crystal optical properties under the given PSD and PHD for each wavelength.

Figure 3 shows the preliminary version of the spectral bulk optical properties of the next-generation ice optical property model at a temperature of 200 K, including the extinction efficiency (top panel), the single-scattering albedo (center panel), and the asymmetry factor (lower panel). For the first time, this optical property model covers the whole spectrum from UV to microwave (0.2–200,000 μm), which can consistently be used for various applications, including broadband radiative transfer, data assimilation, and ice cloud remote sensing. A smooth transition from the geometric optics regime to the Rayleigh regime in these optical properties is seen for the effective radii that are fairly the same order of the magnitude of the spectral wavelength. As the Community Radiative Transfer Model (CRTM) also covers the full wavelength regime from UV to microwave, these full spectral optical properties will be helpful for CRTM to make the ice cloud optical properties consistent among wavelengths.
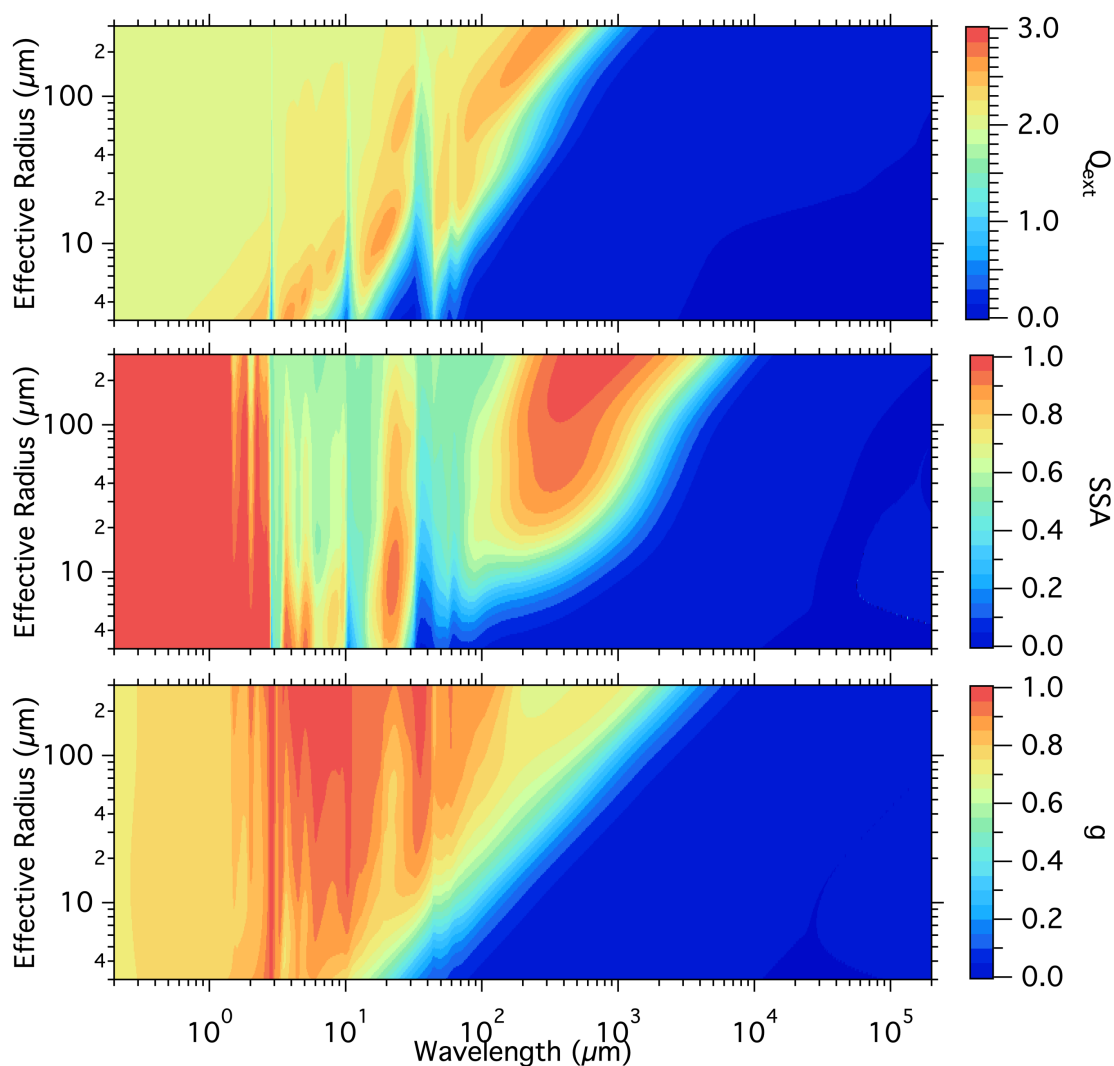
Figure 3. The bulk extinction efficiency (Q_{ext}), single-scattering albedo (SSA), and asymmetry factor (g) of the preliminary version of the next-generation ice optical property model. The wavelength covers from ultraviolet (UV) to microwave, 0.2–200,000 μm, and the effective radii range from 3–300 μm.

As the complex refractive index of ice and dominant ice crystal shapes vary with temperature, we investigate the differences in the optical properties of ice crystals between 200 K and 260 K, as shown in Fig. 4 (200 K minus 260 K). From UV to a thermal infrared wavelength (~10 μm), the differences in the optical properties between 200 K and 260 K are mainly due to the ice crystal shape distributions. At around 260 K, planar ice crystals with high aspect ratios are dominant, which lead to a larger asymmetry factor (i.e., negative values in the asymmetry factor differences shown in Fig. 4). Between the thermal infrared and sub-millimeter wavelengths, the temperature dependence of the complex refractive index of ice and the shape differences lead to differences in the optical properties of ice crystals (Saito et al., 2020).
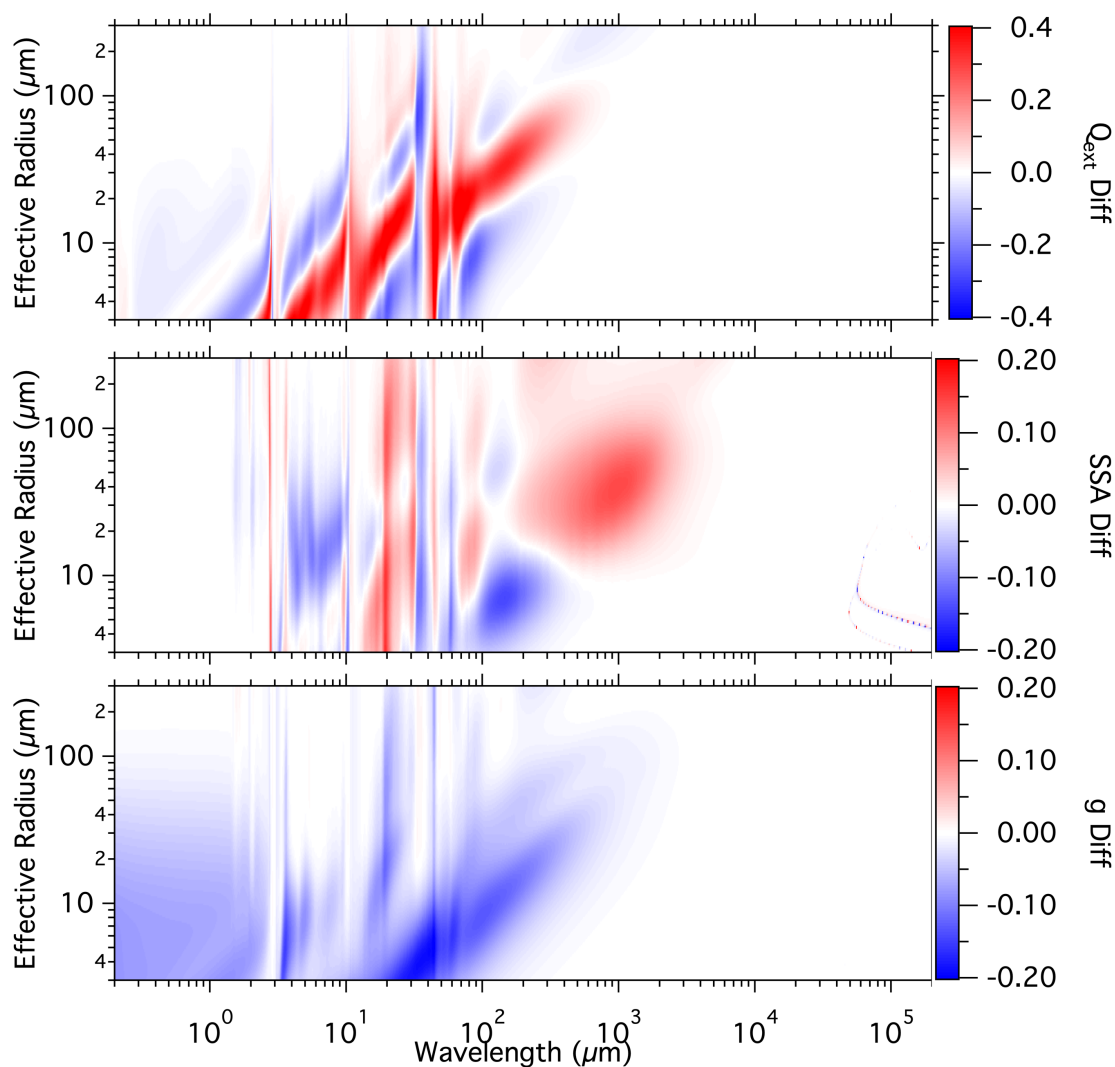
Figure 4. Same as Fig. 3 but for the differences in the optical properties between temperatures 200 K and 260 K.

3. Spectral consistency procedure

The next-generation ice optical property model will be validated through a spectral consistency check based on the optical thickness retrievals using two different methods: The bi-

spectral method based on visible and near-infrared solar reflectances (Nakajima and King, 1990), and the split-window techniques based on the brightness temperature differences among the thermal infrared window channels (Inoue, 1985). The procedure development was completed and tested with the preliminary versions of the next-generation ice optical property model, as shown in Fig. 5.
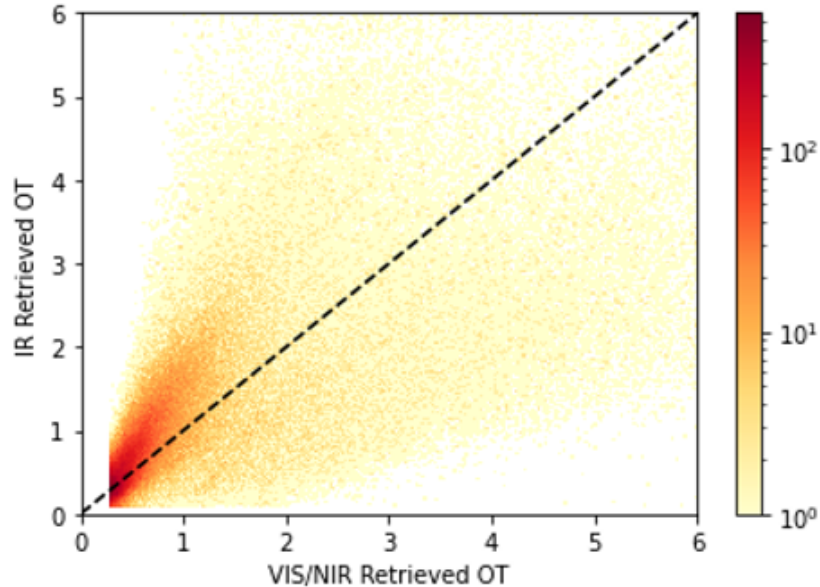
Figure 5. The spectral consistency diagram obtained from an entire granule of GOES-16 observations at 18:00 (UTC) on August 25, 2017.

4. Active-passive consistency procedure

As another solid validation method of an ice optical property model, we will perform the active-passive consistency check using complementary satellite observations from the collocated Cloud-Aerosol Lidar with Orthogonal Polarization (CALIOP) and Moderate-resolution Imaging Spectroradiometer (MODIS) instruments. The CALIOP instrument measures the integrated attenuated backscattering (IAB), which is a function of cloud optical thickness and the lidar ratio of cloud particles, and is analytically derivable from the ice optical property model. The MODIS instrument measures the solar reflectance, that provides the cloud optical thickness based on the bi-spectral method. Figure 6 shows the active-passive consistency diagram based on the current next-generation ice optical property model. Please note that the PGOM simulations, critical to the active-passive consistency, are still ongoing. The active-passive consistency with the next-generation ice optical properties will be further improved once these PGOM calculations are completed.
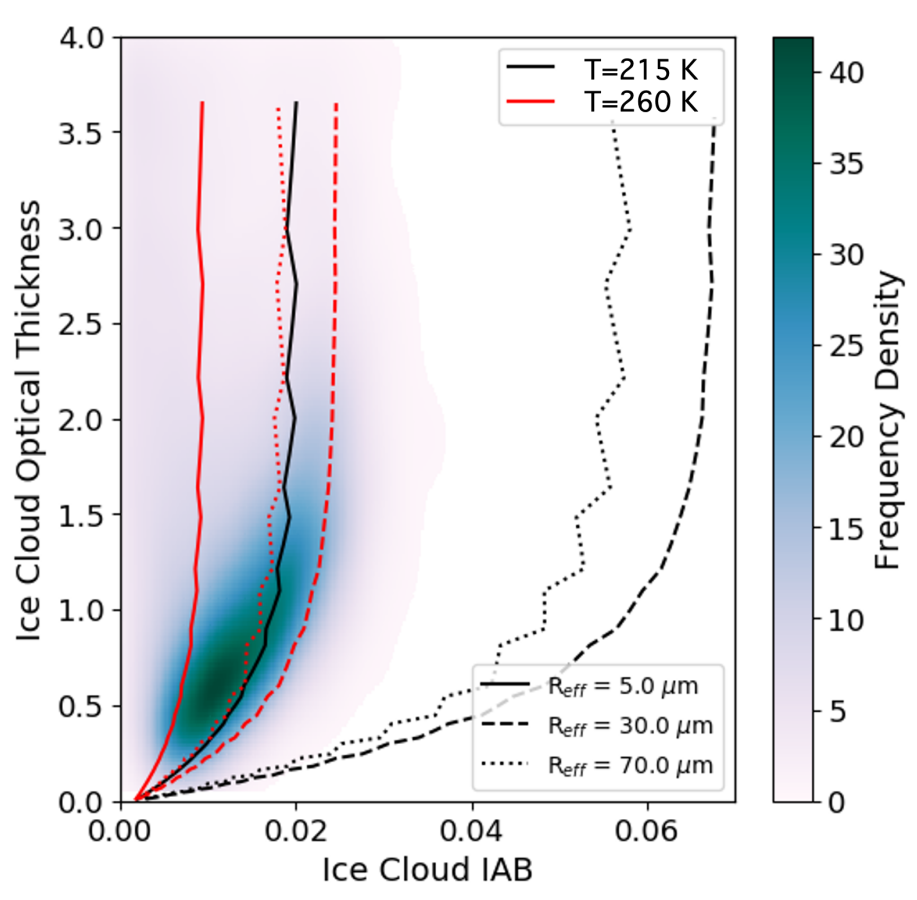
Figure 6. The active-passive consistency diagram using the current next-generation ice optical property model. The vertical axis is the ice cloud optical thickness obtained from the MODIS bi-spectral method.

University of Michigan accomplishments:

5. Further evaluation of the CRTM 2.4.0 for GEOS-17 ABI radiance simulations

The UM team has kept working on the evaluation of the CRTM 2.4.0. As indicated in the previous progress report, we have identified issues in the built-in test temperature profiles in the CRTM 2.4.0. We have corrected the issues since then. To understand the discrepancies for the simulated ABI mid-IR radiances between the CRTM 2.4.0 and MODTRAN5, we have carried out a sequence of sensitivity studies. First, we tested how, under a variety of clear-sky situations, two codes differ for the simulated radiances at the ABI 6.9-µm and 8.4-µm channels. We scale the water vapor content for two typical profiles, one for the tropics (McClatchy et al., 1972) and the other for the US 1976 standard atmosphere. The results are shown as Figure 7. For the 6.9-µm channel (within the H_2O v2 band), the brightness temperature (BT) difference between two codes varies almost linearly with the total column water vapor (TCWV). However, for the 8.4-µm channel (in the mid-IR window region), the BT difference between two codes varies little with the

TCWV. These comparisons suggest that the water vapor spectroscopy treatments in the CRTM 2.4.0 and MODTRAN5 are not consistent across different spectral regions, which can inevitably affect the cloudy-sky radiance simulation.
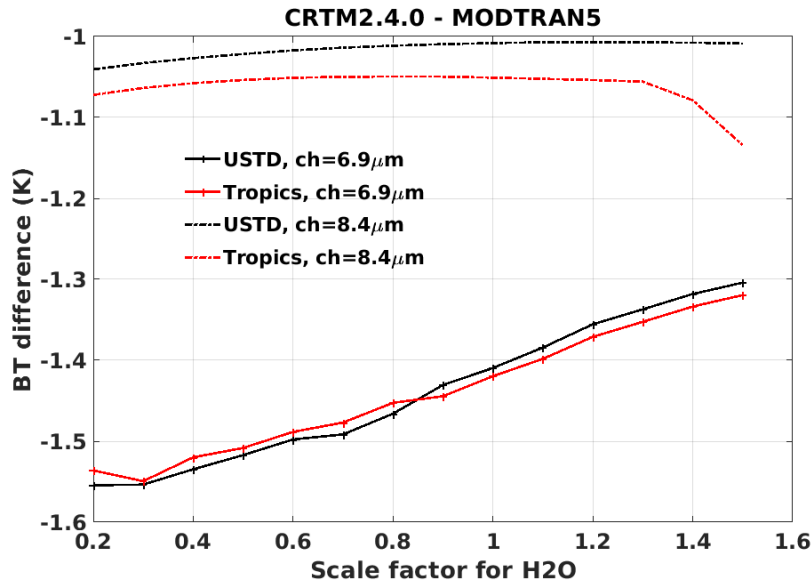
Figure 7. The difference in brightness temperature for a variety of H_2O scaling factors as simulated by CRTM 2.4.0 and MODTRAN5 for two GOES-17 ABI channels, 6.9 μm (solid lines) and 8.4 μm (dashed-dotted lines). The results based on default MODTRAN tropical and USTC 1976 standard atmosphere profile are shown in red and black, respectively. For the tropical profile, the total column water vapor is 4.11 cm when scale factor = 1; for the US 1976 profile, it is 1.42 cm when scale factor =1.

We further examined how the differences between the CRTM 2.4.0 and MODTRAN 5 vary with ice water path (IWP). CRTM 2.4.0 allows cloud existence with any specified water vapor profile, even the relative humidity within the cloud layer is much lower than 100%. While in many other radiation code such as MODTRAN5, cloud layer is automatically set to 100% relative humidity. Such different assumptions can make a difference in simulation studies when the input humidity profiles for the cloud layers do not reach saturation. After ensuring consistent treatments of in-cloud humidity profiles, we compared the simulated BT differences between two codes for a variety of IWP, as shown in Figure 8. The ice cloud was placed between 400 and 500 hPa, i.e., a layer contributing considerably to the TOA radiances at both channels. Figure 8 clearly shows that the simulated BT difference at the 6.9-μm channel varies little with the IWP while the counterpart at the 8.4-μm channel has a strong dependence with the IWP. Such difference cannot be explained by the clear-sky BT differences shown in Figure 9. Thus, these

results suggest that the ice cloud optical properties in the CRTM 2.4.0 must be parameterized in a very different way from the MODTRAN5.
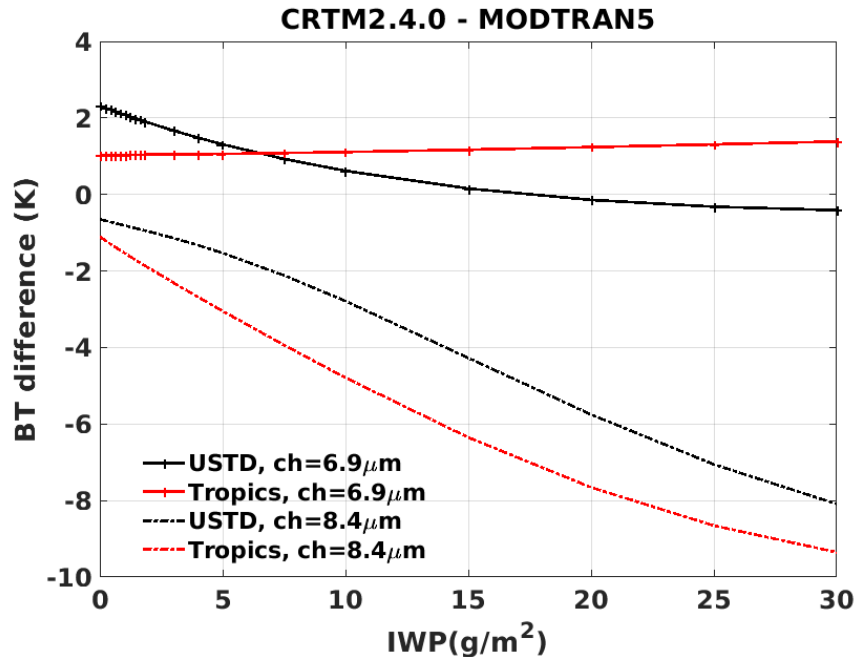
Figure 8. Similar to Figure 8, but for simulated brightness temperature differences between CRTM 2.4.0 and MODTRAN5 for a variety of ice water path. Ice cloud is placed between 400 and 500 hPa.

6. Plans for Next Reporting Period

While we will continue the single-scattering property computations with PGOM during the next six months, we will optimize the particle habit distribution through in-situ observational and theoretical constraints as well as spectral and active-passive consistency checks to finalize the next-generation ice optical property model development. The finalization of the next-generation ice optical property model is scheduled to be delivered to the CRTM team by 31 July 2022. Furthermore, after the next-generation ice optical property model development is completed, we will incorporate the model into CRTM. Moreover, we will further investigate the discrepancies between the CRTM 2.4.0 and MODTRAN5 in ice-cloud simulations and understand the current limitations in the CRTM 2.4.0 for ice-cloud radiance simulation.

References

Baum, B. A., Heymsfield, A. J., Yang, P., & Bedka, S. T. (2005). Bulk scattering properties for the remote sensing of ice clouds. Part I: Microphysical data and models. *Journal of Applied Meteorology*, *44*(12), 1885-1895.

Butterfield, N., P. M. Rowe, E. Stewart, D. Roesel, and S. Neshyba (2017), Quantitative three-dimensional ice roughness from scanning electron microscopy, J. Geophys. Res. Atmos., 122, 3023–3041, doi:10.1002/2016JD026094.

Harrington, J. Y., & Pokrifka, G. F. (2021). Approximate models for lateral growth on ice crystal surfaces during vapor depositional growth. *Journal of the Atmospheric Sciences*, *78*(3), 967-981.

Heymsfield, A.J., Lewis, S., Bansemer, A., Iaquinta, J., Miloshevich, L.M., Kajikawa, M., Twohy, C., & Poellot, MR (2002). A general approach for deriving the properties of cirrus and stratiform ice cloud particles. J. Atmos. Sci. 59, 3–29.

Inoue, T. (1985). On the temperature and effective emissivity determination of semi-transparent cirrus clouds by bi-spectral measurements in the 10 μm window region. J. Meteorol. Soc. Jpn. 63, 88–99, doi:10.2151/jmsj1965.63.1_88.

Loeb, N. G., Yang, P, Rose, F. G., Hong, G., Sun-Mack, S., Minnis, P., Kato, S., Ham, S., Smith, W. L., Hioki, S., & Tang, G. (2018), Impact of ice cloud microphysics on satellite cloud retrievals and broadband flux radiative transfer model calculations. *J. Clim.,* **31,** 1851–1864, https:// doi.org/10.1175/JCLI-D-17-0426.1.

McClatchy, R. A., et al. (1972), Optical properties of the atmosphere, 3rd ed., AFGRL-72–0497, 80 pp., Air Force Geophys. Lab., Bedford, Mass.

Nakajima, T., & King, M. D. (1990). Determination of the optical thickness and effective particle radius of clouds from reflected solar radiation measurements. Part I: Theory. *Journal of the Atmospheric Sciences*, *47*(15), 1878–1893. https://doi.org/10.1175/1520-0469(1990)047<1878:DOTOTA>2.0.CO;2

Neshyba, S. P., B. Lowen, M. Benning, A. Lawson, and P. M. Rowe (2013), Roughness metrics of prismatic facets of ice, J. Geophys. Res. Atmos., 118, 3309–3318, doi:10.1002/jgrd.50357.

Saito, M., Yang, P., Huang, X., Brindley, H. E., Mlynczak, M. G., & Kahn, B. H. (2020). Spaceborne middle-and far-infrared observations improving nighttime ice cloud property retrievals. *Geophysical Research Letters*, *47*(18), e2020GL087491.

Saito, M., Yang, P., Ding, J., & Liu, X., 2021: A comprehensive database of the optical properties of irregular aerosol particles for radiative transfer simulations. *Journal of the Atmospheric Sciences*, in press, https://doi.org/10.1175/JAS-D-20-0338.1

Yang, P., and K. N. Liou, 1996: Geometric-optics-integral-equation method for light scattering by nonspherical ice crystals, *Appl. Opt.*, **35,** 6568–6584.

Yang, P., and K. N. Liou, 1997: Light scattering by hexagonal ice crystals: Solution by a ray-by-ray integration algorithm, *J. Opt. Soc. Amer. A.*, **14,** 2278-2289.

Yang, P., J, Ding, R. L. Panetta, K.-N. Liou, G. W. Kattawar, M. I. Mishchenko, 2019: On the convergence of numerical computations for both exact and approximate solutions for electromagnetic scattering by nonspherical dielectric particles, *Progress In Electromagnetics Research*, 164, 27-61 (invited paper).